# Nanoscale

Accepted Manuscript


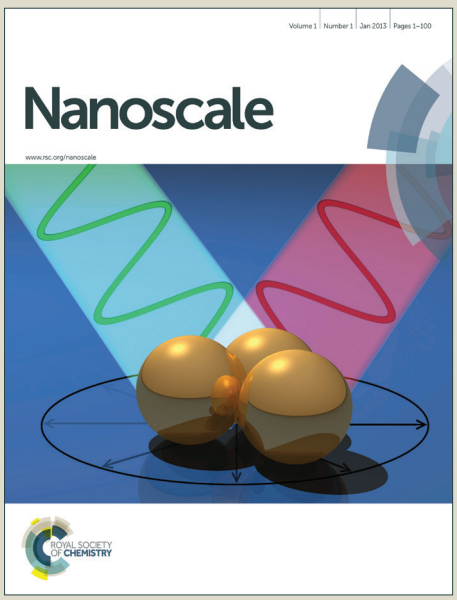





ROYAL SOCIETY OF CHEMISTRY

www.rsc.org/nanoscale

Nano Scale

ARTICLE

# Quantitative Multiplexed Simulated-Cell Identification by SERS in Microfluidic Devices

Received 00th January 20xx,
Accepted 00th January 20xx

DOI: 10.1039/x0xx00000x

www.rsc.org/

M. R. Hoonejani,[a] A. Pallaoro, [b] G. B. Braun,[c] M. Moskovits[b] and C. D. Meinhart[a]

Reliable identification of cells on the basis of their surface markers is of great interest for diagnostic and therapeutic applications. We present a multiplexed labeling and detection strategy that is applied to four microparticle populations, each mimicking cellular or bacterial samples with varying surface concentration of up to four epitopes, using four distinct biotags that are meant to be used in conjunction with surface enhanced Raman spectroscopy (SERS) instead of fluorescence, together with microfluidics. Four populations of 6 µm polystyrene beads, were incubated with different mixtures, "cocktails" of four SERS Biotags (SBTs), simulating the approach one would follow when seeking to identify multiple biomarkers encountered in biological applications. Populations were flowed in a microfluidic flow-focusing device and the SERS signal from individual beads was acquired during continuous flow. The spectrally rich SERS spectra enabled us to separate confidently the populations utilizing principal component analysis (PCA). Also, by using classical least squares (CLS), we were able to calculate the contributions of each SBT to the overall signal in each of the populations, and showed that the relative SBT contributions are consistent with the nominal percentage of each marker originally designed into that bead population, by functionalizing it with a given SBT cocktail. Our results demonstrate the multiplexing capabilities of SBTs in such potential applications as immunophenotyping.

## Introduction

The ability to target and easily detect multiple biomarkers (multiplexing) on the surface of cells is important for applications such as immunophenotyping, which is commonly employed for discriminating among different cell types for the diagnosis of diseases such as cancer and bacterial infections.[1-5] The use of several biomarkers for the phenotypic characterization of certain cellular subgroups based on their surface expression increases the sensitivity, reliability and robustness of such methods.[6] Fluorescence labeling is the predominant technology for bioimaging and cytometry and has been proven to be a highly valuable technique, suitable for quantitative analysis and even single molecule detection, under appropriate conditions.[7] However, *multiplexed* fluorescence imaging and cytometry are often challenging, given the broadness of the fluorescence emission spectrum, limiting the number of fluorophores with non-overlapping emission spectra that can be used simultaneously. Moreover, multiple excitation lasers are often needed, which increases the cost and complexity of such instruments.

Surface enhanced Raman scattering (SERS) is a highly enhanced form of Raman spectroscopy which has been used in such broad applications as chemical detection, diagnostics, and imaging.[8-11] SERS-active nanosystems may have emission cross-sections rivaling those of fluorescence, implying that well-crafted SERS biotags are in principle possible that are almost as bright as fluorescence biotags. Consequently, SERS biotags potentially offer an alternative approach to fluorescence biotags that addresses some of its shortcomings. For example, the narrow SERS bandwidths offer much greater facility in deconvoluting the various contributors to a composite SERS spectrum resulting from the simultaneous use of multiple labels. Existing chemometric analytic methods can be used to quantify the contributions of the various sharp SERS peaks belonging to the various Raman reporter molecules to the overall SERS spectrum. Additionally, since it is the SERS-active metallic nanostructure that is being excited and not the individual reporter molecule,[12] the SERS spectrum of all of the labels can be excited using a single red wavelength (as we do here) laser, or even one emitting in the near infrared, that wavelengths do little cell damage and reduces the propensity for autofluorescence.[13] Furthermore, SERS provides an unparalleled level of sensitivity, up to single molecule detection.[14] *In vitro* SERS imaging and detection of cancer cells and pathogens have been previously reported, [9,15-18] however, only a few examples of multiplexed SERS labeling of cells in vitro can be found in the literature,[11,19-22] and very few in

[a] *Department of Mechanical Engineering, University of California, Santa Barbara, CA 93106, USA.*
[b] *Department of Chemistry and Biochemistry, University of California, Santa Barbara, CA 93106, USA*
[c] *Cancer Research Center, Sanford Burnham Prebys Medical Discovery Institute, 10901 N. Torrey Pines road, La Jolla, CA 92037, USA.*
Electronic Supplementary Information (ESI) available: Detailed methods and experimental procedures on device fabrication and SBTs synthesis and assembly, additional characterization of SBTs, and PCA analysis See
DOI: 10.1039/x0xx00000x

conjunction with microfluidics.[23] We reported previously the synthesis of silver nanoparticle-based SERS Biotags (SBTs)[24] that are exceptionally bright and stable in biological media and used them in a "two-color" configuration for the detection of cancer cells based on the quantification of surface receptor expression.[11,23] We also used them for the local pH measurement in single cells at subcellular resolution.[25]

Here, we introduce a strategy for the identification of micron-size particles functioning as cell proxies flowing in a microfluidic channel, based on their SERS spectral signatures. Four populations of polystyrene beads (diameter, 6 μm) were synthesized and are uniquely identified. Each population is labeled with a cocktail of SBTs containing up to four different Raman reporter molecules ("colors") varying in the ratios of each of the four "colors" in each of the populations **(Fig. 1A)**, with one SBT always being at 25% of the total and used as common marker **(Fig. 1B)**. The SBT cocktail compositions were designed to simulate a typical immunophenotyping scenario, where four cell populations are labeled based upon the different expression levels of four surface biomarkers.

interrogating them with a 633 nm laser beam that simultaneously excited all the SBTs bound to the bead surface **(Fig. 1C)**. The spectra were analyzed using principal component analysis (PCA) to qualitatively distinguish among the four populations and by classical least squares (CLS) for quantification of the contribution of each SBT to the overall SERS signal from single beads.

## Results and Discussion

The SBTs are small clusters (predominantly dimers) of silver nanoparticles (~45 nm in diameter) encapsulated in poly(vinylpyrrolidone) for stability.[24] A modified bovine serum albumin (see methods for details) imparts further stability and offers a handle for bioaffinity conjugation. SBTs are then infused with the Raman reporter molecules and are finally decorated with SVA-PEG-biotin to promote binding to the streptavidin coated polystyrene beads. Bead populations were incubated with the SBT cocktails and were injected into the

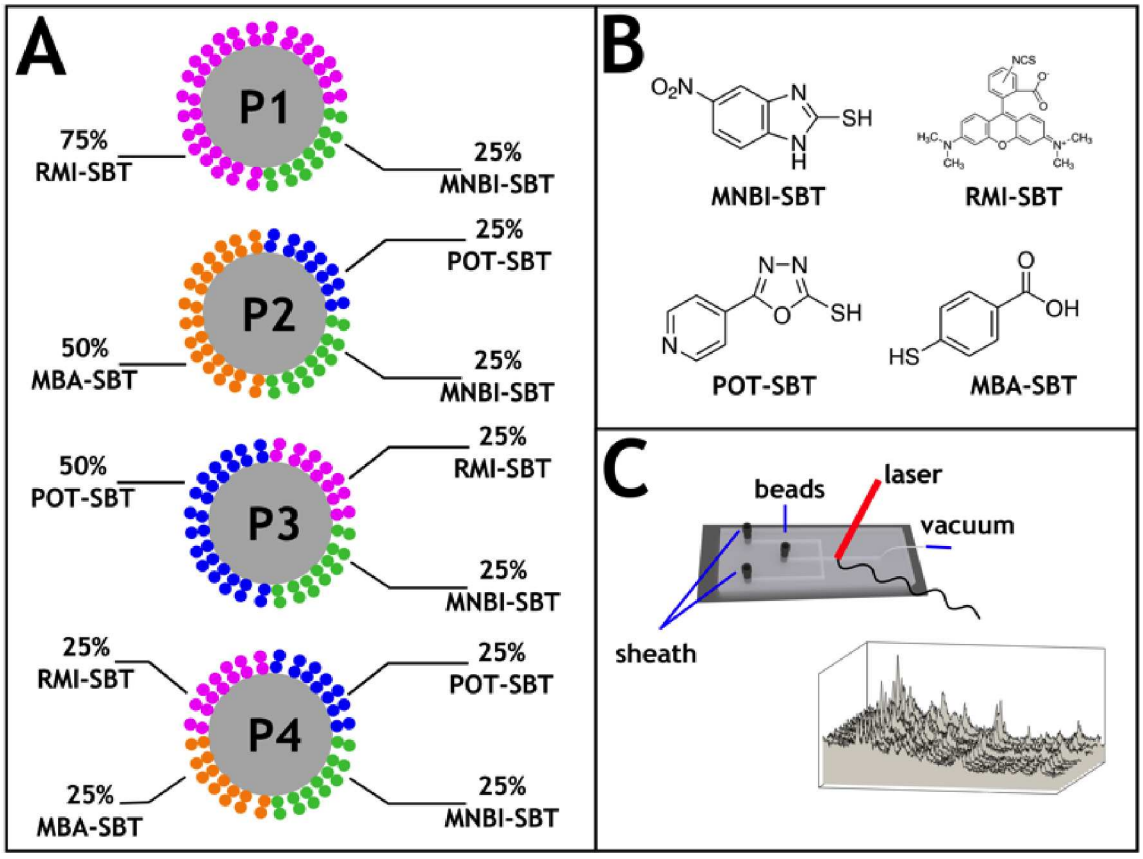


Fig. 1. (A) The composition of each SBT cocktail that was incubated with beads in creating each of the four populations. Population 1 is incubated with a mixture of 25% MNBI-SBT and 75% RMI-SBT. Population 2 cocktail is composed on 25% MNBI-SBT, 25% POT-SBT, and 50% MBA-SBT. The cocktail introduced to population 3 consists of 25% MNBI-SBT, 25% RMI-SBT, and 50% POT-SBT. Lastly, the fourth population is incubated with an equal mix of all four tags. Note that there is 25% MNBI-SBT in all the populations as an onboard universal tag. (B) Molecular structures of the four Raman reporter molecules that were infused in the SBTs. The reporters were selected carefully based on their spectral features. (C) A schematic of the microfluidic/SERS strategy. The tagged beads were injected into a flow-focusing microfluidic device and their SERS signal was acquired at the interrogation site every 100-150 ms. The recorded spectra were then analyzed using CLS and PCA.

Nano Scale

ARTICLE

microfluidic device after blocking any free streptavidin with biotin and washing unbound SBTs by centrifugation. Characterization and TEM images of the beads carrying SBTs were published by us previously.[26]

The four Raman reporters used for this study were 4-mercaptobenzoic acid (MBA), tetramethylrhodamine isothiocyanate mixed isomers (RMI), 5-(4-pyridyl)-1,3,4-oxadiazole-2-thiol (POT), and 2-mercapto-5-nitrobenzimidazole (MNBI) (Fig. 1B). The Raman reporters were selected based on two factors: (i) at least one Raman band in the spectrum of each reporter molecule is unique in the sense that it does not overlap with any strong band in the spectra of any of the others, (ii) the overall SERS intensity from equal concentrations of SBTs of the selected tags is approximately comparable. In this case none of the reporter molecules are resonant with the 633nm excitation laser. After assembly of the SBTs, their concentration was normalized based on their UV-Vis spectra (Fig. S1).

The microfluidic flow-focusing device[27] possesses one inlet for beads, one inlet for the sheath buffer, an outlet connected to vacuum, and an interrogation region just downstream of the junction where the side flows meet the beads stream. The relative flow rates in the various channels are dictated by the geometry of the channels including widths and length at various points along the flow. The flow rates were set such that each bead resides within the focused laser beam for 5-8 ms for interrogation as it flows across the device. The SERS measurements in the microfluidic device were conducted using a LabRAM Aramis spectrometer (Horiba Jobin-Yvon, Kyoto, Japan) using a 633 nm laser and a 10x objective lens. A spectrum collected over 20 ms nominal detector exposure time was acquired every 100-150 ms.

To eliminate the spectra that do not contain useful SERS information, we applied a filtering PCA (fPCA) algorithm on the basis of which spectra containing only peaks associated with PDMS were eliminated. The fPCA model for each bead population is a 1-PC (principal component) model, which contains the combined spectral features of the SBT cocktail corresponding to that particular population in addition to the peaks associated with PDMS. Beads whose SERS spectra are rich in contributions from the SBTs register high values for fPC1, while PDMS-only spectra score zero or very close to zero. An example of fPCA is shown in Fig. S2. Since all peaks of interest in all populations reside between 280-1800 $cm^{-1}$, only this range was used in the analysis. Finally, the spectra were preprocessed by baseline subtraction, normalization and mean centering.

The goal of this study is two-fold, in the first instance, it is to develop the spectroscopic, microfluidic and chemometric analysis tools with which to correctly identify to which of the four populations a bead crossing the laser beam belongs; and, secondly to correctly determine (i.e. to determine within tolerable limits) the relative concentrations of the four SBTs resident on the interrogated bead. We begin by plotting the average SERS spectra of the four populations against the spectra obtained from single SBTs (Fig. 2). All populations have 25% nominal contribution from MNBI-SBT. The 831 $cm^{-1}$ peak and 1337 $cm^{-1}$ shoulder, associated with MNBI-SBT, are present in the average spectra of all populations (green bands). The RMI-SBT peaks such as 1655, 1363, 1509, 500, and 282 $cm^{-1}$ are present in all populations, except population 2 whose SBT cocktail did not contain RMI-SBT (violet bands). The prominent SERS bands associated with MBA-SBT (1591 and 1083 $cm^{-1}$) can only be seen in populations 2 and 4, which were originally incubated with MBA-SBT (orange bands). And finally, peaks associated with POT-SBT (1621, 1553, and 1022 $cm^{-1}$) appear in all populations except population 1 whose SBT cocktail of labels did not contain POT-SBT (blue bands). It should be mentioned that peaks associated with PDMS Raman signature can also be seen in regions with small contributions from SBTs. For example, the 489 $cm^{-1}$ PDMS peak, which overlaps with RMI-SBT slightly, appears in population 1 average spectrum as a shoulder to the left of the RMI-SBT peak. Also, the 708 $cm^{-1}$ peak is present consistently in all the average spectra from populations.

**Population Discrimination using PCA**

Principal component analysis (PCA) is a powerful qualitative method for determining variations and trends in a dataset.

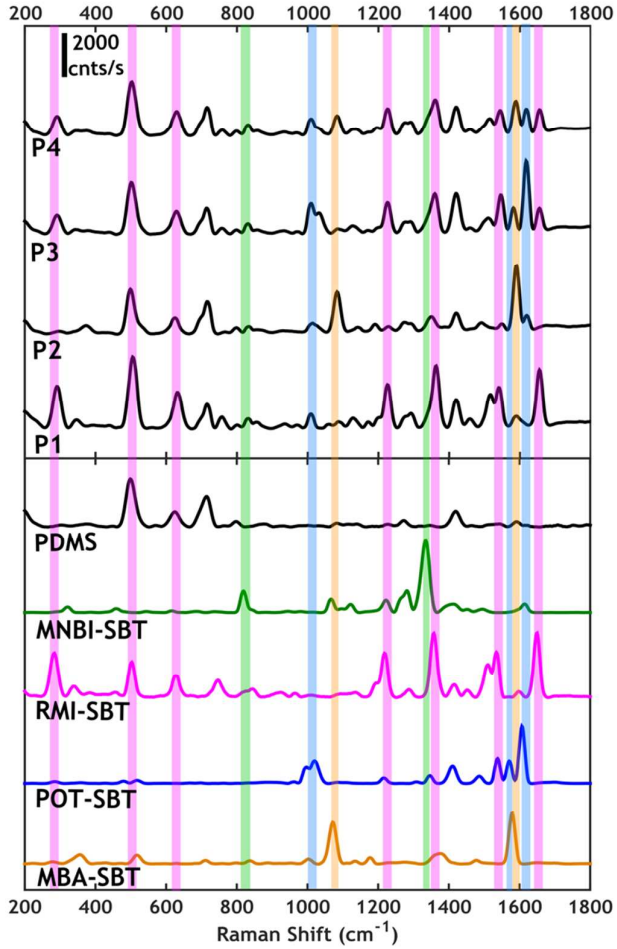


**Fig. 2.** Average SERS spectra of the four bead populations (top) compared to the SERS spectra of the individual SBTs (bottom). Unique bands of each SBT are denoted by ribbons of the same color: green for MNBI-SBT, violet for RMI-SBT, orange for MBA-SBT, and blue for POT-SBT. The SERS peaks from each of the individual pure components are present in the average spectra from populations in agreement with the nominal composition of the SBT cocktail introduced to that population originally.

Using PCA, we can lower the dimensions of a set of spectra from hundreds of wavenumbers to a few principal components (PCs). Each spectrum in the dataset can then be approximated as a linear combination of these PCs. In carrying out this analysis the spectra from all four populations were analyzed using PCA as a single dataset. A 3-component model (shown in Fig. 3B) was generated based on the preprocessed and filtered spectra from individual populations. PC1 shows positive peaks associated with RMI-SBT (1655, 1363, 1226, and 282 $cm^{-1}$) and negative peaks associated with MBA-SBT (1591 and 1083 $cm^{-1}$) and POT-SBT (1621, 1553, and 1022 $cm^{-1}$). This is reflected in the PC1-PC2 scores map presented in Fig. 3A as population 1, which is labeled with 75% nominal RMI-SBTs, and shows positive PC1 scores whereas population 2, not labeled with RMI-SBTs, scores negative in PC1. PC2, on the other hand, appears to have positive contributions from POT-SBT and negative contributions from MBA-SBT. In the PC1-PC2 map, this can be seen as population 3 with 50% nominal contribution from POT-SBTs, which has positive PC2 score. PC3 appears to indicate the overall signal from all populations and has peaks corresponding to RMI-SBT, MBA-SBT, and POT-SBT; as such, PC3 scores do not show a significant variation among the populations (Fig. S3). Note that none of the peaks associated with MNBI-SBT are present in the principal components, as expected: MNBI-SBT is an onboard reference label common to all the populations, and as a result its contribution is subtracted from the spectra in the mean centering preprocessing step.

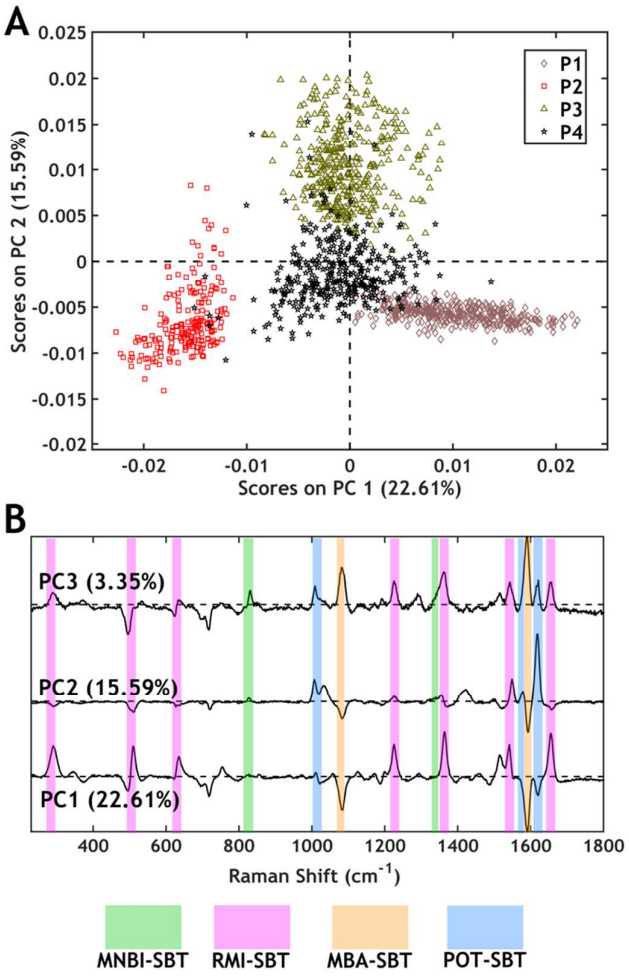


**Fig. 3.** Summary of principal component analysis results. (A) PC1-PC2 scores map for the four populations shows separation between the populations. Each point in this plot corresponds to the PC1 and PC2 scores returned by PCA for a single bead spectrum. PC1 appears to be separating population 1 and 2 from the rest of the mix. Similarly, PC2 separates population 3 from the rest of the populations. (B) PCs calculated by PCA. PC1 appears to have positive contribution from RMI-SBT peaks (violet markers) and negative contributions from MBA-SBT and POT-SBT (orange and blue markers, respectively). PC2 on the other hand, has positive peaks associated with POT-SBT and negative peaks associated with MBA-SBT. PC3 shows positive peaks from RMI-SBT, MBA-SBT, and POT-SBT and negative contributions from PDMS.

**SBT Contribution Quantification using CLS**

PCA provides clear separation of the four populations. However, PCA is not quantitative information, which is required when it is necessary to determine the relative magnitudes of the various contributions of tags to the overall signal, for example, in order to determine quantitatively the

extent of surface biomarker expressions on cells. Quantifying tag contributions and comparing them to the original SBT cocktail combinations would also indicate the extent to which the SBTs bind to the beads.

Quantitative analysis was carried out using classical least squares (CLS), which assumes the spectra from the beads in each population to be a linear combination of the SERS spectra of the four SBTs. For each spectrum, CLS scores were calculated, yielding the coefficients in the linear combination corresponding to the relative contributions of each SBT to the overall SERS signal. This analysis was carried out only over the range 800-1800 $cm^{-1}$, which includes most of the SERS bands from SBTs and excludes prominent PDMS bands.

Normalized CLS scores of each SBT for all the populations are shown in **Fig. 4**, along with the nominal percent composition of the cocktail combinations, shown for convenience. **Fig. 4A** shows the contribution of SBTs to the spectra from population 1, with the highest mean value from RMI-SBT (75.0±0.7%), 15.5±0.3% from MNBI-SBT and almost no contribution from MBA-SBT and POT-SBT (6.5±0.1% and 2.9±0.1%, respectively), which is consistent with the nominal

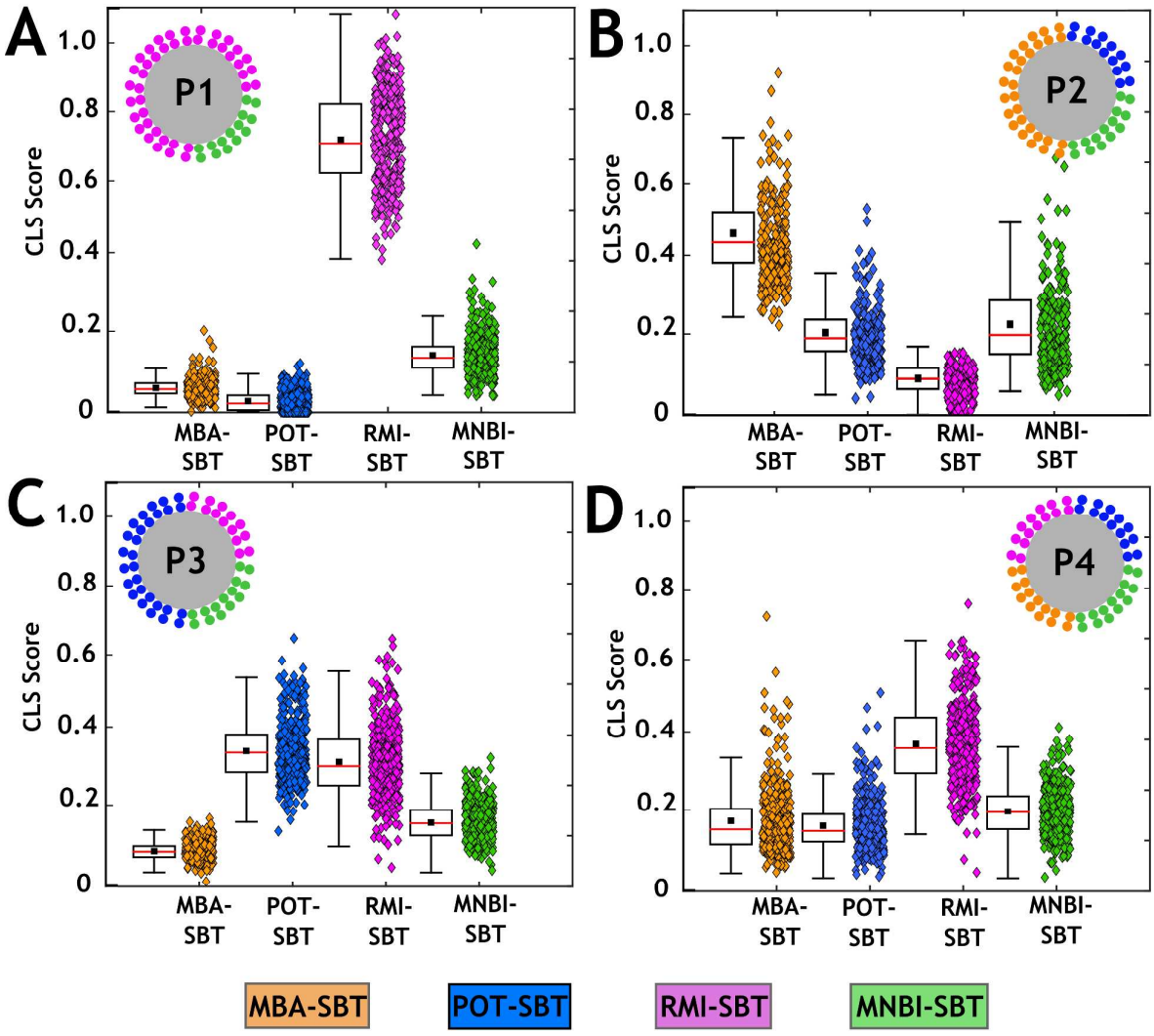


Fig. 4. Classical least square (CLS) results. The classical least squares technique was used to quantify the SBT contribution to the spectra from each population. (A), (B), (C), and (D) show normalized CLS scores (coefficients) for populations 1 to 4. CLS scores corresponding to the SBTs calculated contributions have been plotted for each population. The relative SBT scores calculated by CLS are in agreement with their nominal values in the SBT cocktail used to synthesize the respective bead population. Slightly higher RMI-SBT can be explained by the larger SERS cross-section of this tag compared to others. In the box plots, the black dot shows the mean value for each distribution, the middle red line shows the median and top and bottom lines of the box show the 75 and 25 percentile values, respectively. Also, the whiskers show upper and lower adjacent values which is 3×IQR (Interquartile Range). For convenience, the SBT combination of different populations is also shown in their respective panel.

Nano Scale

ARTICLE

relative composition of the SBT cocktail used to create population 1 (75% RMI-SBT and 25% MNBI-SBT). The CLS scores for population 2 are shown in **Fig. 4B**. For this population, the analysis estimated the POT-SBT and MNBI-SBT to have similar mean contributions of 21.4±0.5% and 23.4±0.6%, respectively. Also, MBA-SBT in this population has an average contribution of 47.1±0.8% and RMI-SBT 9.3±0.2% in agreement with the population 2 SBT cocktail which nominally consists of 50% MBA-SBT, 25% POT-SBT, and 25% MNBI-SBT, respectively. In **Fig. 4C**, the average calculated contributions of SBTs in population 3 are 10.2±0.1% for MBA-SBT, 37.7±0.4% for POT-SBT, 34.7±0.6% for RMI-SBT, and 18.0±0.3% for MNBI-SBT. Comparing these numbers to the nominal SBT contributions in this population (50% POT-SBT and 25% RMI-SBT and MNBI-SBT), one notes that RMI-SBT has a somewhat higher CLS score, which is likely due to RMI having a slightly larger SERS cross-section over that of POT. Finally, in population 4 with 25% nominal contribution from each SBT, the average CLS scores are 19.4±0.6%, 18.1±0.4%, 40.5±0.6%, and 22.0±0.4% for MBA-SBT, POT-SBT, RMI-SBT, and MNBI-SBT, respectively. All the SBTs have comparable contributions in this population, which is consistent with the nominal values except for, again, the relatively higher RMI-SBT score. Normalized CLS scores and the nominal SBT contributions are summarized in **Table S1**.

The box plots in Fig. 4 show the statistics of the CLS scores calculated for the four SBTs and populations. The SEM (standard error of the mean) of the calculated SBT scores for each population is smaller than 5%. Boxes of SBT contributions are very well separated across populations where the nominal percentages are different. To test whether the calculated differences among the four populations are statistically significant based on their SBT contributions, a nonparametric analysis of variance test (Kruskal–Wallis) was performed on the CLS results for each SBT across populations and yielded a p-value < 0.001, which shows the populations are statistically different based on their SBT contributions.

## Conclusion

A multiplexed SERS labeling and detection strategy was demonstrated by employing four microbead samples (populations) that functioned as cell-proxies. Each population was labeled with a different cocktail of SERS Biotags (SBTs) consisting of a mixture of four tags and differing in the nominal percent composition, resulting in varying relative SBTs surface concentration, simulating multiple biomarker scenarios that one might encounter in actual immunophenotyping. The four populations were probed using SERS as the microbeads flowed continuously through a microfluidics device that allowed individual beads to be interrogated. The overall SERS spectra from the individual beads were analyzed using two chemometric methods: principal component analysis and classical least squares. PCA, a qualitative method, successfully showed that the populations separate into four distinct groups. While classical least squares (CLS), a quantitative method, indicated that the contribution of each SBT to the overall SERS signal from beads (calculated with SEM < 5%) corresponded to the nominal SBT population that was present in the SBT cocktail that was used to functionalize the beads in each of the four populations with SBTs. The successful categorization of the four bead populations (Kruskal-Wallis test, $p < 0.001$) and quantification of each of the SBTs bound to the surface of the beads is possible because of the rich nature of the SERS spectrum, which consists of many narrow bands.

## Acknowledgements

This work is in part supported by the Institute for Collaborative Biotechnologies through contract no. W911NF-09-D-0001 from the U.S. Army Research Office. The content of the information does not necessarily reflect the position or the policy of the Government, and no official endorsement should be inferred. Financial support from the University of California Cancer Research Coordinating Committee is also gratefully acknowledged. The fabrication was undertaken in the University of California, Santa Barbara Nanofabrication Facility, part of the National Science Foundation-funded National Nanofabrication Infrastructure Network.

## Notes and references

1 J. Hulkkonen, L. Vilpo, M. Hurme and J. Vilpo, *Leukemia*, 2002, **16**, 178–185.
2 P. Dalerba, S. J. Dylla, I.-K. Park, R. Liu, X. Wang, R. W. Cho, T. Hoey, A. Gurney, E. H. Huang, D. M. Simeone, A. A. Shelton, G. Parmiani, C. Castelli and M. F. Clarke, *Proc. Natl. Acad. Sci. U S A*, 2007, **104**, 10158–10163.
3 R. Scatena, P. Bottoni and B. Giardina, *Biochim. Biophys. Acta*, 2013, **1835**, 129–143.
4 S. Hanash, F. Brichory and D. Beer, *Disease Markers*, 2001, **17**, 295–300.
5 K. Reinhart, M. Bauer, N. C. Riedemann and C. S. Hartog, *Clinical Microbiology Reviews*, 2012, **25**, 609–634.
6 C. LOMBARDI, G. F. TASSI, G. PIZZOCOLO and F. DONATO, *Chest*, 1990, **97**, 639–644.
7 C. Joo, H. Balci, Y. Ishitsuka, C. Buranachai and T. Ha, *Annu.*

*Rev. Biochem.*, 2008, **77**, 51–76.
8 C. Andreou, M. R. Hoonejani, M. R. Barmi, M. Moskovits and C. D. Meinhart, *ACS Nano*, 2013, **7**, 7157–7164.
9 R. A. Alvarez-Puebla and L. M. Liz-Marzán, *Small*, 2010, **6**, 604–610.
10 K. C. Bantz, A. F. Meyer, N. J. Wittenberg, H. Im, Ö. Kurtuluş, S. H. Lee, N. C. Lindquist, S.-H. Oh and C. L. Haynes, *Phys. Chem. Chem. Phys.*, 2011, **13**, 11551–11567.
11 A. Pallaoro, G. B. Braun and M. Moskovits, *Proc. Natl. Acad. Sci. U S A*, 2011, **108**, 16559–16564.
12 M. Moskovits, *Phys. Chem. Chem. Phys.*, 2013, **15**, 5301–5311.
13 U. Mahmood and R. Weissleder, *Mol. Cancer Ther.*, 2003, **2**, 489–496.
14 K. Kneipp, Y. Wang, H. Kneipp, L. T. Perelman, I. Itzkan, R. R. Dasari and M. S. Feld, *Phys. Rev. Lett.*, 1997, **78**, 1667–1670.
15 M. M. Harper, K. S. McKeating and K. Faulds, *Phys. Chem. Chem. Phys.*, 2013, **15**, 5312–5328.
16 J. V. Jokerst, Z. Miao, C. Zavaleta, Z. Cheng and S. S. Gambhir, *Small*, 2011, **7**, 625–633.
17 C. T. Nguyen, J. T. Nguyen, S. Rutledge, J. Zhang, C. Wang and G. C. Walker, *Cancer Lett.*, 2010, **292**, 91–97.
18 I. Freitag, C. Matthäus, A. Csaki, J. H. Clement, D. Cialla-May, K. Weber, C. Krafft and J. Popp, *J. Biomed. Opt.*, 2015, **20**, 055002–055002.
19 C. M. MacLaughlin, N. Mullaithilaga, G. Yang, S. Y. Ip, C. Wang and G. C. Walker, *Langmuir*, 2013, **29**, 1908–1919.
20 J. P. Nolan, E. Duggan, E. Liu, D. Condello, I. Dave and S. A. Stoner, *Methods*, 2012, **57**, 272–279.
21 L. Rodriguez-Lorenzo, L. Fabris and R. A. Alvarez-Puebla, *Anal. Chim. Acta*, 2012, **745**, 10–23.
22 K. Gracie, E. Correa, S. Mabbott, J. A. Dougan, D. Graham, R. Goodacre and K. Faulds, *Chem. Sci.*, 2014, **5**, 1030–1040.
23 A. Pallaoro, M. R. Hoonejani, G. B. Braun, C. D. Meinhart and M. Moskovits, *ACS Nano*, 2015, **9**, 4328–4336.
24 G. B. Braun, S. J. Lee, T. Laurence, N. Fera, L. Fabris, G. C. Bazan, M. Moskovits and N. O. Reich, *J. Phys. Chem. C*, 2009, **113**, 13622–13629.
25 A. Pallaoro, G. B. Braun, N. O. Reich and M. Moskovits, *Small*, 2010, **6**, 618–622.
26 A. Pallaoro, M. R. Hoonejani, G. B. Braun, C. D. Meinhart and M. Moskovits, *J. Nanophotonics*, 2013, **7**, 3092.
27 T. Stiles, R. Fallon, T. Vestad, J. Oakey, D. W. M. Marr, J. Squier and R. Jimenez, *Microfluid. Nanofluid.*, 2005, **1**, 280–283.